New rate equation model to describe the stabilization of displacement damage by hydrogen atoms during ion irradiation in tungsten

M. Pečovnik[*a], E. A. Hodille[b], T. Schwarz-Selinger[c], C. Grisolia[d] and S. Markelj[a]

[a]*Jožef Stefan Institute, Jamova cesta 39, 1000 Ljubljana, Slovenia*
[b]*Department of Physics, University of Helsinki, P. O. Box 43, FI-00014, Finland*
[c]*Max-Planck-Institut für Plasmaphysik, Boltzmannstrasse 2, D-85748 Garching, Germany*
[d]*CEA, IRFM, F-13108 Saint Paul Lez Durance, France*

Abstract

The effect of deuterium (D) presence on the amount of displacement damage created in tungsten (W) during high-energy W-ion irradiation is investigated. For this purpose, we have performed modelling of experimental results where W was sequentially or simultaneously irradiated by 10.8 MeV W ions and exposed to 300 eV D ions. A novel displacement damage creation and stabilization model was newly developed and introduced into the MHIMS-Reservoir (Migration of Hydrogen Isotopes in MaterialS) code. It employs macroscopic rate equations (MREs) for solving the evolution of solute and trapped D concentrations in the material.

The new displacement damage creation and stabilization model is based on spontaneous recombination of Frenkel pairs and stabilization of defects that are occupied by D atoms. By using the new model, we could successfully replicate the measured D depth profiles and D thermal desorption data, where a higher defect concentration was observed when D was present during W irradiation as compared to when no D was present. For this we utilized parameters, which include the number of distinct defect types, the de-trapping energies of their fill-levels, their saturation concentrations and their probability for stabilization if they contain a D during the W-ion irradiation. To successfully replicate the experimental results three distinct defect types were needed with several fill-levels. By comparing the de-trapping energies of the defect fill-levels with data available from the literature, the defect types were identified as single-vacancies, small vacancy clusters and large vacancy clusters. The effect of D presence was found to be largest in single vacancies as its concentration increased by about a factor of three, while the concentration of small vacancy clusters increased by about a factor of two. Large vacancy clusters were found to be largely unaffected as they showed very little increase in concentration when D was present.

1. Introduction

Understanding the interaction between the plasma and the surrounding wall materials of future fusion reactors and plasma is of crucial importance when trying to achieve a controlled fusion reaction which yields more energy than is necessary to heat the plasma. This interaction consists of several aspects ranging from wall material erosion to irradiation and transmutation of the material because of 14.1 MeV neutron irradiation originating from the D-T fusion reaction ($D^+ + T^+ \rightarrow He^+$ (3.5 MeV) + neutron (14.1 MeV)). Also a very important aspect is the retention of hydrogen isotopes in the wall of the reactor, namely radioactive tritium. This so-called tritium inventory must be maintained and controlled inside a future reactor below a specific limit for safe and fuel-efficient reactor operation. Taking all these things into consideration one of the most promising materials is tungsten (W) as it exhibits low hydrogen isotope (HI) solubility which leads to low intrinsic HI retention. It also has a very high melting point which is needed to resist the high fluxes of particles reaching 10^{24} part/m^{2}s [1] and intense heat loads up to 10 MW/m^2.

The before mentioned 14.1 MeV neutrons will not only cause transmutation of W, but also displacement damage in the tungsten crystal lattice in the amount of several displacements per atom (dpa) per year throughout the material [2, 3]. In the context of heavy ion or neutron irradiation, displacement damage means displacement of W atoms from their equilibrium position in the crystal lattice and creation of lattice defects. The defects created by such displacement damage act as strong trapping sites for hydrogen isotopes as they exhibit de-trapping energies that are higher than the energy we associate with diffusion of hydrogen between interstitial sites. As predicted by rate equation modelling tritium inventory in these traps will be the main contribution to the entire tritium inventory of the W plasma facing components [4].

Because neutrons with energy as high as 14.1 MeV are created only in such complex experimental conditions present in a fusion reactor, there is an obvious lack of laboratory experiments that are able to study the evolution of defects. Furthermore, not only is it difficult to create neutron damage in samples used for hydrogen isotope retention studies, but one must also realize that during the creation of defects in realistic tokamak conditions, the wall will also be bombarded by various other particles from the plasma and will be subjected to elevated temperatures.

Neutrons produce displacement damage in the crystal lattice in cascades. First a neutron impacts a tungsten atom in the crystal lattice which is knocked out of its place and a significant energy transfer occurs. This energetic W ion then causes further displacement damage in the material in cascades. Because of the nature of such displacement damage creation it has been shown that damaging the material by energetic heavy ions is a good proxy for neutron damaging [5], excluding effects such as transmutation and in-wall helium production. A special case that is typically used to simulate the displacement damage caused by neutrons is irradiation with high energy W ions (also named self-ion irradiation or self-damaging) as such irradiation does not introduce any chemical impurities into the material which could skew the results of the experiment.

Usually experiments that study hydrogen isotope retention in tungsten are done in a sequential scheme, where the samples are first heavy ion irradiated at a certain temperature up to a specific dpa level and then loaded with deuterium (D) atoms or ions [6, 7]. To study the evolution of defects at elevated temperatures in sequential experiments, annealing at high temperatures is used after the irradiation process [8, 9]. Such experiments are not adequate for studying realistic conditions in a fusion reactor, where the tungsten material is simultaneously subjected to very high temperatures, high hydrogen isotope particle fluxes and is also irradiated by neutrons. There may be some synergistic effects present between these parameters in the processes of defect creation and annihilation, like defect stabilization by the presence of hydrogen isotopes during high temperature annealing [10], so a more complete laboratory experiment is needed to be able to address this. By successfully describing the processes that occur in benchmark experiments, extrapolations can be used to predict the defect evolution in the much harsher fusion relevant conditions.

The extrapolations of these benchmark experiments are usually done by using simulations based on macroscopic rate equation models encapsulated in codes like MHIMS [11], TESSIM [12] and TMAP [13]. These codes use the classical D-defect interaction picture where a defect can trap only one D atom and its de-trapping energy is defined by the type of defect it is trapped in. However, recent DFT results [14, 15, 16] showed that defects like vacancies can trap several HIs and that the de-trapping energy of the HIs from the defect is defined by the number of trapped HIs. This breakthrough in understanding of the D-defect interaction (herein named fill-level dependent model) has been included in macroscopic rate-equation codes like MHIMS-R(eservoir) [17] and TESSIM-X [18]. Both the fill-level-dependent model and the classical model behave equally well when trying to replicate experiments where the conventional sequential scheme of heavy ion irradiation and post-irradiation D exposure is used. The necessity of the fill-level dependent model was only highlighted when experiments studying low temperature H/D isotope exchange were carried out [18, 19].

Past investigations of synergistic effects between D and He during irradiation were done on various steels that are foreseen to be used in future tokamak reactors [20-25]. Their main focus was in the temperature regime where significant swelling of the material was observed. The investigations showed that the simultaneous triple exposure of D – He – Fe, where the Fe is responsible for the neutron-like displacement damage, showed a synergistic effect on cavity formation and growth, as cavity density was higher in the case of triple ion irradiation, compared to dual He – Fe irradiation [20, 21]. Also an increased size of the formed cavities was observed in the case of triple ion irradiation. These effects were further enlarged in the case of high concentrations of D and He present in the sample during the Fe irradiation. A review and an attempt on modelling of these effects was done by Marian *et al.* [25]. Their work produced some qualitatively good results, but the underlying mechanisms remained unclear.

Understanding the mechanisms that lead to synergistic effects during irradiation is of vital interest to the fusion-relevant materials community. Because of the similarities in the properties of different fusion-relevant materials like Fe and W, understanding these processes in one such material would surely contribute to the overall understanding also in other similar materials.

Recently, experiments that tied together the relevant parameters of HI inventory in W have been performed [10]. There, as a first step the samples were irradiated at elevated temperatures by 10.8 MeV W ions to a displacement damage level of 0.47 dpa and later loaded by low-energy D atoms to decorate the created defects. This served as a benchmark experiment to determine the influence of W irradiation temperature on the amount of displacement damage created during such an irradiation. The experiment showed that the amount of displacement damage created depends strongly on the W irradiation temperature. As one would expect the amount of displacement damage created decreases with increasing temperature, because at higher temperatures self-interstitial W atoms and vacancies become more mobile which promotes defect annihilation. As a second step to a more complete description, the samples were W irradiated in the same manner as before while also being simultaneously subjected to a 0.28 eV/D atom beam, to study a possible synergistic effect of HI presence on the creation of defects. The experiment showed that there is a defect stabilizing effect by the presence of D as the amount of displacement damage created in the simultaneous case was systematically higher. This set of experimental data was successfully described by Hodille et al. [26] using the MHIMS code.

In this paper we model the results of a succeeding experimental study where W samples were irradiated with 10.8 MeV W ions to a displacement damage dose of 0.35 dpa at various temperatures and exposed to 300 eV/D ions instead of atoms up to a fluence of 2.8×10^{23} D m^{-2} [27]. To describe this new experiment, we have used and upgraded the MRE model in the MHIMS-R code so it is able to describe the process of displacement damage creation by energetic heavy ions with or without the presence of D [26]. The upgraded model has two free parameters, the saturation concentrations of each defect type, with which we can describe the sequential experiment, and the probability of stabilization of a D-filled defect with which we can describe the results of the simultaneous experiment.

2. Experiment

Two complementary sets of experiments are modelled in this paper as they provide valuable insights into how displacement damage is created in W and on possible synergistic effects between the W ion irradiation and the D present in the sample. Here, only a short overview of the experimental procedures and conditions will be given. More details can be found in Ref. [27]. In both experiments polycrystalline 99.997 wt. % hot-rolled tungsten samples were used. The samples were irradiated by 10.8 MeV W ions up to a fluence of 1.0×10^{18} W/m^2 creating a displacement damage dose of 0.35 dpa$_{KP}$ at the damage peak (Kinchin-Pease calculation, 90 eV displacement damage energy, evaluating the "vacancy.txt" output). The samples were W irradiated at different temperatures ranging from 300 to 1000 K, but in this work we limit ourselves to the 300 – 800 K range as the increase of D concentration observed in the simultaneously W irradiated sample at a temperature of 1000 K cannot be explained by our stabilization model. This is because our stabilization model relies on defect stabilization by trapped D and at a 1000 K according to the modelling no D should be trapped in the defects made by the W irradiation. Despite this fact, a two-times increase in D concentration is experimentally measured when the irradiation is done simultaneously compared to if it is done sequentially. In [27] this was explained by the possibility of vacancy clustering.

The 300 K W irradiation case served as a comparison to our previous work where D atom retention in self-ion irradiated W was studied [6, 8, 10, 28] and to other experiments that employ room temperature W ion irradiation for displacement damage creation [29-31].

The displacement damage during the specific W-ion irradiation procedure was decorated using a 300 eV/D ion beam with a flux of 1.9×10^{18} D m^{-2}s^{-1} for 39 hours at 450 K amounting to a D fluence of 2.8×10^{23} D m^{-2} to decorate the created defects. An additional sample was exposed only to the 300 eV/D ion beam up to a fluence of 2.8×10^{23} D m^{-2}, to serve as a control sample for the possible displacement damage created by the energetic D ion beam and to determine the amount of natural defects present in the sample.

The D depth profiles and the D desorption spectra, which are the input data for our simulation, were measured using the Nuclear Reaction Analysis (NRA) and Thermal Desorption Spectroscopy (TDS) techniques, respectively.

2. 1. Sequential W-D experiment

In order to study displacement damage creation when W samples are irradiated with an energetic 10.8 MeV W ion beam at different W irradiation temperatures, the so-called sequential W-D experiment was used, where no D was present during W-ion irradiation. Considering the simulation, the sequential experiment can be divided into three parts:

(1) W self-ion irradiation at different temperatures (300 K, 450 K, 600 K, 800 K) with a W flux of $\Gamma_W = 9.73 \times 10^{13}$ W m^{-2}s^{-1} for four hours,

(2) Exposure to D ions, loading with $\Gamma_D = 1.9 \times 10^{18}$ D m^{-2}s^{-1} for 39 hours at 450 K amounting to a D fluence of 2.8×10^{23} D m^{-2} to decorate the created defects; D depth profile measured at the end of exposure,

(3) A TDS measurement with an oven heating ramp equalling 3 K/min.

Between parts (1) and (2) a cooling period was set ranging from 1 to 2 hours without D flux. The temperature of the sample during the cooling in vacuum was monitored during the experiment and the measured temperature time dependence was used. Similarly, between steps (2) and (3) the sample was cooled to 300 K where it was left for 1 hour in a "storage" phase which simulated the waiting time between the experiment and the TDS measurement.

2. 2. Simultaneous W/D-D experiment

To study the effect of D presence on displacement damage creation by a W ion beam, the so-called simultaneous W/D-D experiment was used. For the simulation the experiment is again divided roughly into three phases:

(1) Simultaneous W/D exposure at different temperatures (450 K, 600 K, 800 K) with $\Gamma_W = 9.73 \times 10^{13}$ W m^{-2}s^{-1} and $\Gamma_D = 1.9 \times 10^{18}$ D m^{-2}s^{-1} for four hours; D depth profile measured at the end of exposure,

(2) Further ion loading with $\Gamma_D = 1.9 \times 10^{18}$ D m^{-2}s^{-1} for 39 hours at 450 K amounting to a D fluence of 2.8×10^{23} D m^{-2} to decorate the created defects, D depth profile measurement;

(3) A TDS measurement with an oven heating ramp equalling 3 K/min.

Again appropriate cooling periods were included between parts of the experiment.

3. Simulation

To simulate the sequential W-D and the simultaneous W/D-D experimental results [27] we used a variant of the MHIMS (Migration of Hydrogen Isotopes in MaterialS) code [11]. The code is based on a 1D rate equation model which is used to simulate D depth distributions and D desorption spectra in experiments where HI retention and transport mechanisms are of interest. We used a variant of the code which uses the here named fill-level dependent model, named MHIMS-R [17]. The D fill-level dependent model of the D-defect interaction assumes that each type of defect in the W lattice can trap several D atoms. The energy that is needed to de-trap a D atom from the defect depends on the number of D atoms trapped in the defect and on the type of defect as shown by Density Functional Theory (DFT) [14-16]. For comparison, the classical model of the D-defect interaction assumes that each defect can trap only one D atom and that the de-trapping energy for D is only defined by the defect type. The general parameters of the MHIMS-R code that will be used in this paper are listed in Table 1.

Table 2: Summary of the general parameters that we use in our simulations.

Symbol	Description	Value	Reference
ρ	Atomic density of W	6.3×10^{28} m^{-3}	
D(T)	Diffusion coefficient	$1.9 \times 10^{-7} \exp\left(\frac{-0.2\ eV}{k_B\ T}\right)$ m^2 s^{-1}	[14]
n_{TIS}	Concentration of TIS	$6 \times \rho$	[14]
λ	Jumping distance between TIS	110 pm	[14]
ν_0	Pre-exponential factor of de-trapping	10^{13} s^{-1}	[14]

The original MHIMS code uses a defect creation model that is suitable to describe experiments where the dynamics of defect creation are important [11, 26]. The concept is based on a model of displacement damage creation by energetic HI ions in W proposed by Ogorodnikova [32], which itself is based on spontaneous recombination of Frenkel-pairs first introduced by Duesing *et al.* [33]. The model is designed in a way so it can reproduce the saturation of D concentration above a desired displacement damage dose (dpa) through saturation of the defect concentration. The displacement damage dose where saturation of D and consequently defect concentrations was observed is somewhere between 0.1 and 0.3 dpa [7, 29, 34, 35]. The model of displacement damage creation, as was included in the MHIMS code can be written as:

$$\frac{dn_i(x,t)}{dt} = \frac{\Gamma \, \eta_i \, \theta(x)}{\rho^2}\left[1 - \frac{n_i(x,t)}{n_{i,max}}\right] \qquad (1)$$

Here $n_i(x,t)$ (at.%) is the time and spatially dependent defect concentration of trap type i and Γ (m^{-2} s^{-1}) is the flux of particles that are causing displacement damage to the material, here W ions. $\theta(x)$ (dimensionless) is the depth distribution of primary displacement damage created by implanted W ions as calculated by SRIM [36], shown in Fig. 2a. $n_{i,max}$ (at.%) determines the saturation concentration of defect type i and η_i(m^{-1}) is the probability for defect creation and corresponds to the number of defects a irradiating ion produces per unit length. Concentration of a certain species in our context is defined as the ratio of the atomic density of a certain species to the atomic density of tungsten.

Previously, as a first test case the MHIMS model was used to describe the displacement damage created by exposure of W samples to 200 eV/D ions [11]. After this it was upgraded so it could also describe the process of displacement damage creation with energetic heavy ions. This upgrade was put to use by Hodille *et al.* [26] when modelling the experiment described in the introduction where W samples were irradiated by energetic W ions at various temperatures with or without D atom exposure [26]. But the model did not include an explicit dependence on D presence yet, so the sequential and simultaneous experiments were modelled simply by changing the defect saturation concentrations - $n_{i,max}$.

To use the established MHIMS displacement damage creation model in combination with the fill-level D-defect interaction we had to first implement it into the MHIMS-R code, which previously contained no displacement damage creation model. During the implementation of the old model (equation 1) into MHIMS-R we have also used the opportunity to upgrade it with a novel stabilization mechanism, which is for the first time proposed and implemented here. It takes the presence of D during W irradiation fully into account. Our modified model, that will be used to describe the experimental results from [27] governs the time evolution of the concentration of the i-th type of defect and is described with the following equation:

$$\frac{dn_i(x,t)}{dt} = \frac{\Gamma \, \eta_i \, \theta(x)}{\rho^2}\left[1 - \frac{n_i(x,t)}{n_{i,max}}\left(1 - \alpha_i \frac{n_i(x,t) - n_i^0(x,t)}{n_i(x,t)}\right)\right] \qquad (2)$$

As can be seen, the model is exactly the same as above (Eq. 1) except for the term in the round parenthesis. The addition of this novel stabilization mechanism explicitly takes into account how D affects the defect creation process by including the dynamics of D diffusion and trapping into the equation. Here α_i (dimensionless) is the degree of stabilization and $n_i^0(x,t)$ (at.%) is the depth distribution of defect concentration of defect type i that has no trapped D. This means $n_i(x,t) - n_i^0(x,t)$ is the depth distribution of concentration of D-occupied defect type i (with at least one D). The model is appropriate to describe experiments where some kind of displacement damage creation (heavy ion irradiation, high energy HI irradiation, neutron irradiation) is the dominating process as the concept of annihilation is only implicitly taken into account through defect concentration saturation. Therefore, the model is not suitable for studying the process of annealing.

3. 1 Kinetic de-trapping

We have also included kinetic de-trapping into MHIMS-R after its importance was elucidated in Ref. [37]. Kinetic de-trapping is the process where an impacting heavy ion recoils a trapped D atom from its defect through a kinetic energy transfer. It is an additional source term for the solute D concentrations.

In the MHIMS-R code the kinetic de-trapping process was included by adding an additional frequency term for de-trapping due to W-D energy transfer during a collision - v_{KD} (s^{-1}) - to the de-trapping rate constant $v_i(T)$:

$$v_i(T) = v_0 e^{-\frac{E_{t,i}}{kT}} + v_{KD} \qquad (3)$$

The first term, $\nu_0 \exp\left(-\frac{E_{t,i}}{kT}\right)$ is the well-known first order thermal desorption rate of HI from a defect with $\nu_0 = 10^{13}$ s^{-1} being the de-trapping attempt frequency and $E_{t,i}$ the de-trapping energy. The second term is the kinetic de-trapping frequency which is parametrized as:

$$\nu_{KD} = \frac{\Gamma\,\eta_{KD}\,\theta(x)}{\rho} \tag{4}$$

Here Γ (m^{-2}s^{-1}) is the flux of W ions, ρ (m^{-3}) is the density of tungsten and $\theta(x)$ (dimensionless) is the calculated normalized primary displacement damage distribution of a W ion beam with a specific energy, which is calculated by SRIM [36] and is shown in Fig. 2a for our 10.8 MeV W ions. The same $\theta(x)$ is used for both displacement damage creation and for kinetic de-trapping as Schwarz-Selinger *et al.* showed in Ref. [37] that the shapes of the depth distribution of displaced W fraction and recoiled D are almost the same. The distributions as drawn in Ref. [37] only differ in the absolute amounts because displacement energies for W and D are different, being 90 eV and 1 eV, respectively. To take this into account we introduce η_{KD} which is the probability of an impinging W ion to recoil a trapped D per unit depth. It is considered as a fitting parameter in our model. We assumed its value to be $\eta_{KD} = 7.62 \times 10^{13}$ m^{-1} as this produces the best fits of the simulation to our experimental data. The same η_{KD} was used for all defect types and fill-levels, although strictly speaking it should change in accordance with the de-trapping energies of D.

Our choice of parametrization of D kinetic de-trapping defined in equation 4 means that we have assumed no significant energy transfer to occur between the kinetically de-trapped D and the impinging W ions. This is represented by the fact that the kinetically de-trapped D enters the solute at exactly the point where it was recoiled.

The effect of kinetic de-trapping is that it decreases the steady-state occupation ratio of all the defects which in turn means that diffusion of D into the bulk is faster and the normally sharp D diffusion front is smeared out. Therefore, possible synergistic effects between the D present in the sample and the W ion beam are expected to be seen deeper than if no kinetic de-trapping would be present.

3. 2 Boundary conditions

Usually when ions are implanted deep into the bulk of the material it is assumed that the surface desorption is rate limited by the diffusion to the surface, because the time-scale of diffusion from deep in the bulk to the surface are much larger than the time-scale of D desorption from the surface. This means it is assumed that a D atom that comes to the surface of the material from the bulk desorbs immediately [38]. Therefore, the Dirichlet boundary condition on the surface is assumed and implemented by setting the D surface concentration to zero - $c_m(x = 0) = c_m(x = L) = 0$. Here, c_m (at. %) is the concentration of solute D particles and L the thickness of the sample.

As the D ions are implanted directly into the bulk, the implantation flux is modelled as a volume source of solute D in the bulk. The distribution of the source is calculated with SRIM [36] and is modelled as a Gaussian distribution with a projected mean range of 5 nm and a lateral straggle of 2.9 nm for the 300 eV/D ion exposure.

3. 3 Choice of fill-level dependent model

In this subsection we will discuss why we have chosen to use the fill-level dependent D-defect interaction picture. At first we used the MHIMS code with the classical HI trapping picture where only one HI can be trapped per defect and the defect de-trapping energy is dependent only on the defect type, coupled with the novel displacement damage creation and stabilization model. For that simulation five different de-trapping energies were included to describe the TDS data. In the classical picture these five de-trapping energies are interpreted as different defect types. The evolution of the defect concentrations with W

irradiation temperature of some of these defects was very similar. This lead us to think that these de-trapping energies with similar behaviour were actually part of the same defect type and that they correspond to different filling levels of this defect. If this observation was indeed true then the entire desorption kinetics of the experiment could be described by several different defect types with several fill-levels, which motivated us to use the more complex fill-level dependent picture of D trapping in the MHIMS-R code [17].

Based on the above described observation we have chosen to use three distinct defect types with two, two and one fill-level respectively. This choice was not affected by any fill-level data available in the literature for various defect types, as the number of defects, number of their fill-levels and fill-level de-trapping energies were optimized to produce the best fit possible instead of optimizing them to the existing literature data. This ensured a level of independence of our results and ensured additional simulation bias was not introduced. The de-trapping energies of the found fill-levels were only later compared to values from the literature to try and identify the various defect types. This will be discussed in more detail in the discussion section.

4. Simulation results

We will first outline the general steps we have taken when fitting a D depth profile and a D desorption spectrum for a single sample. By changing the number of distinct defects, the number of their fill-levels and their respective de-trapping energies and by changing the ratios between saturation concentrations of all the defects we first reproduce the general shape of the D desorption spectra. The defect depth distribution is not a free parameter as it is given by $\theta(x)$. After this we adjust the absolute values of the saturation concentrations for all the defects, while maintaining the ratios between them, to fit the D depth profile and the local retained amount of D in the samples which we get by summing up the area under the measured D depth profile.
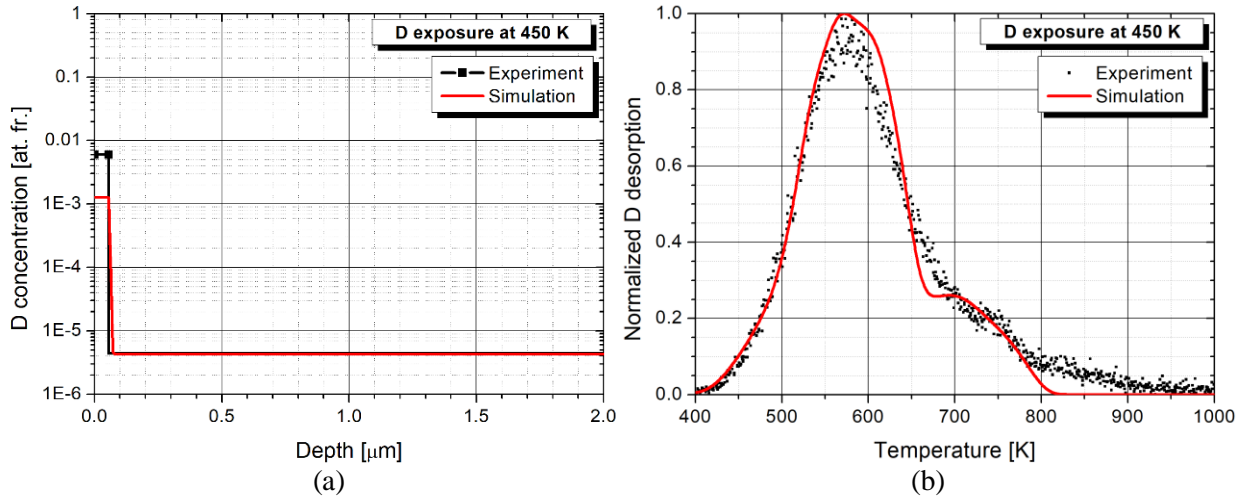

Figure 1: The D depth profile obtained after the D ion 300 eV/D exposure is shown on the left (a) and the corresponding D desorption spectra on the right (b). The experimental data is plotted with dots and the simulation with a line.

First we simulate the exposure of the control sample that was exposed only to the 300 eV/D ion beam with a flux of 1.9×10^{18} D/m²s for 39 hours at 450 K to determine the effect of the D exposure on D retention in the sample without irradiating it with W ions. The deconvolution of the NRA proton spectra revealed a rather high amount of deuterium at the surface as shown in Fig 1a. The actual D concentration might be badly defined by the limited depth resolution and can also be attributed to surface adsorption. Deeper in the sample the D concentration quickly reduces to values of 4×10^{-6} at. fr. and can be attributed to

intrinsic defects. From the D desorption spectrum shown in Fig. 1b, we can see that most of the D is released in a single peak at a temperature of around 580 K and that a small desorption shoulder is visible at around 730 K.

As we use the Dirichlet boundary conditions we cannot describe the increase of retained D near the surface with chemisorption, therefore we use a single defect as a proxy which has a high concentration near the surface while at larger depths its concentration is zero. By our choice, the depth to which it extends is 50 nm and has a concentration equalling 4.2×10^{-4} at. fr. with several de-trapping energies (1.62 eV, 1.72 eV, 1.84 eV). Comparison of desorption energies with the de-trapping energies from our proxy defect is impossible, because de-trapping from our proxy defect is a first order process, while the desorption of D_2 molecules from a surface is a second order process [39]. Still, the de-trapping energies of the proxy defect can be considered as a rough estimate of the surface desorption energies. The D retention in the bulk is fitted with a single intrinsic defect with a concentration equalling 8.5×10^{-7} at. fr. and with 5 fill-levels with de-trapping energies (1.28, 1.41, 1.72, 1.84, 2.00) eV which we attribute to be natural defects present in the sample.

This set of parameters produced the best fit of the D depth profile and D desorption spectra, which can be seen in Fig. 1a and Fig. 1b, respectively. The D depth distribution is fitted reasonably well as can be seen in Fig. 1a as a pronounced peak of D concentration is observed near the surface that is due to D trapping in our chemisorption-proxy defect. Also the low D concentration tail extending deep into the bulk is well reproduced. As can be seen in Fig. 1b, the D desorption spectrum is also well replicated by the simulation. By determining the effects of the D ion beam exposure itself we have established that the effects of the exposure on D retention, compared to the process of displacement damage creation with self-ions is negligible, which is why we do not implement any surface proxy defect or intrinsic defects in further simulations.

After determining the effect of the D ion beam exposure itself, let us also shortly discuss our choice for the free fitting parameters of the simulation that will be kept constant throughout simulating both the W/D and W/D-D experiments. First we define our choice for the probability of displacement damage creation - η. We have used a value of 1.5×10^9 m^{-1} to simulate the experimental results because this choice produces a flat defect distribution throughout the entire damage layer at displacement damage doses around 0.30 dpa, which is considered as an upper limit of displacement damage dose [29]. Probabilities that are smaller than 1.5×10^9 m^{-1} would produce a D depth profile that is not yet completely flat because defect saturation would not yet occur in the entire damage depth and the defect depth distribution is expected to still somewhat resemble the SRIM [36] calculated primary displacement damage depth distribution. We justify the use of the same η for all defect types by the fact that in [29] the ratios of the different TDS peaks were not dependent on the W fluences (damage doses) used, which means that the probabilities for creation are roughly the same for all defect types.

Another important set of free parameters are the number of distinct defect types and the de-trapping energies from their fill-levels. As the thermal desorption spectra for both sets of experiments show the same desorption peak distribution [27], these were the determined defects and de-trapping energies that describe them well:

- Defect I with 2 filling levels (1.35 eV, 1.46 eV)
- Defect II with 2 filling levels (1.68 eV, 1.86 eV)
- Defect III with 1 filling level (2.10 eV)

By keeping η the same for all W irradiation temperatures and defect types and by keeping the de-trapping energies mostly the same for both experimental sets we could reproduce the experimental results very well.

Moreover, we normalized the D desorption spectra of the sequential and simultaneous cases separately to the highest D desorption observed in both series for both the experiment and the simulation. The reason for this is because the D ion beam was inhomogeneous across the W irradiated area as was discussed in detail in [27] and the D depth profiles were measured at the sample position where the maximum D concentration was found.

4. 1 Simulation of sequential W-D experiment

First we simulate the W-D experiment where the sample was sequentially W ion irradiated and afterwards exposed to 300 eV/D ions. The comparison between the simulation and experiment is shown in Fig. 2a and Fig. 2b for all W-ion irradiation temperatures.
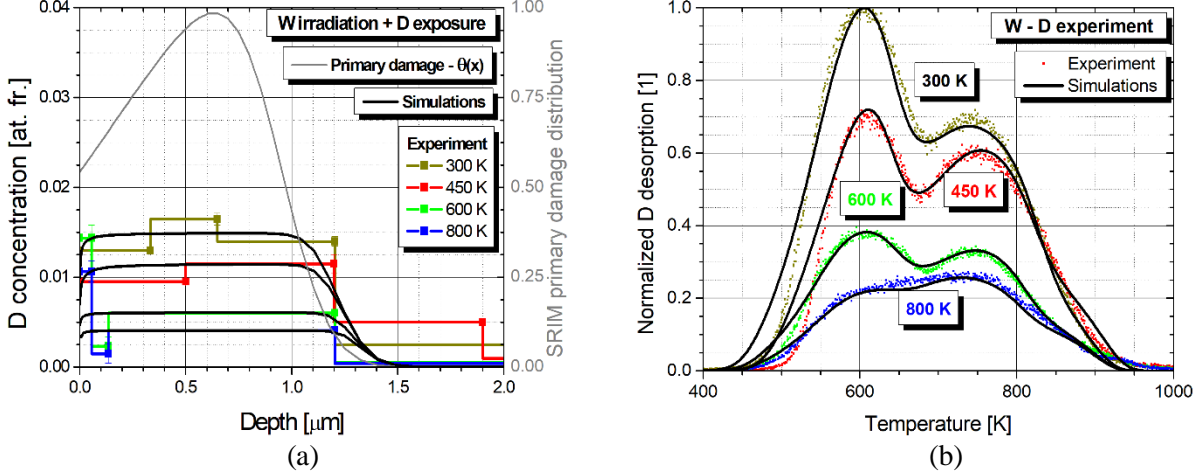

Figure 2: Sequential W self-ion irradiation and D ion decoration: (a) A comparison between the experimental and simulation D depth profiles for four W irradiation temperatures. (b) A comparison between the experimental and simulation D desorption spectra for all four W irradiation temperatures. The spectra were normalized to the maximum desorption of the W sample irradiated at 300 K.

The depth distribution of D is fitted very well for all temperatures, which signifies that the probability for displacement damage creation η combined with the displacement damage distribution function acquired from SRIM [36] were good choices. Their combined use successfully reproduces the depth distribution of the major part of D retained in each sample. The only real mismatch is in the D depth profile for the sequentially W irradiated and D loaded sample at 450 K (drawn in red in Fig. 2) which exhibits a deep D concentration tail which is not reproduced by the simulation. This long step of D going deeper into the sample is a consequence of the fact that the NRA measurement used has a depth resolution of around 0.6 µm at a depth of 1.5 µm. This means the NRA spectrum deconvolution process that produces the D depth profiles could not take a narrower and higher step around 1.2-1.4 µm which is more realistic for a 10.8 MeV W ion irradiation scenario. In summary the relatively high D concentration deep in the 450 K sample is due to the fitting process and is most probably not a real feature one should strive to reproduce.

We would like to stress that the correct D depth distribution is very important for correctly determining the de-trapping energies and the trap concentrations as the D depth distribution of a trap has a non-negligible effect on the shape of the D desorption spectra [40].

The two peak structure of the D desorption spectra is reproduced very well by the simulation as can be seen in Fig. 2b. By changing the saturation concentrations of the three defect types we were able to also reproduce the different ratios of the two desorption peaks at different W irradiation temperatures. To quantify the quality of the fit of the TDS spectra (figure 2b), the reduced chi square is used. It is defined as:

$$\chi^2_{red} = \frac{1}{N-1} \sum_{i=1}^{N} \frac{\left(\Gamma_i^{sim} - \Gamma_i^{exp} \right)^2}{\sigma_i^2}$$

N is the number of points in the experimental desorption spectra. Γ_i^{exp} is the experimental desorption flux at a temperature T_i and similarly Γ_i^{sim} is the simulation desorption flux at T_i. σ_i is the experimental error of desorption at temperature T_i. It was determined directly from the D desorption measurement count rates, assuming that the relative error follows Poisson statistics meaning the experimental relative error at a temperature T_i is directly proportional to the square root of the number of counts measured at that temperature. Another experimental error that we must consider comes from the relative error for the particle fluxes derived from the drift and fluctuations of the quadrupole signal while dosing a constant amount of D_2 into the chamber with a calibrated leak bottle. This error was experimentally determined to be about 1-2 %. The χ_{red}^2 calculation was limited to TDS temperatures between 550 and 900 K where 90 % of retained D was desorbed. The calculated χ_{red}^2 are listed in Table 2 for each desorption spectrum. Their values are close to 1 which confirms the quality of the fit.
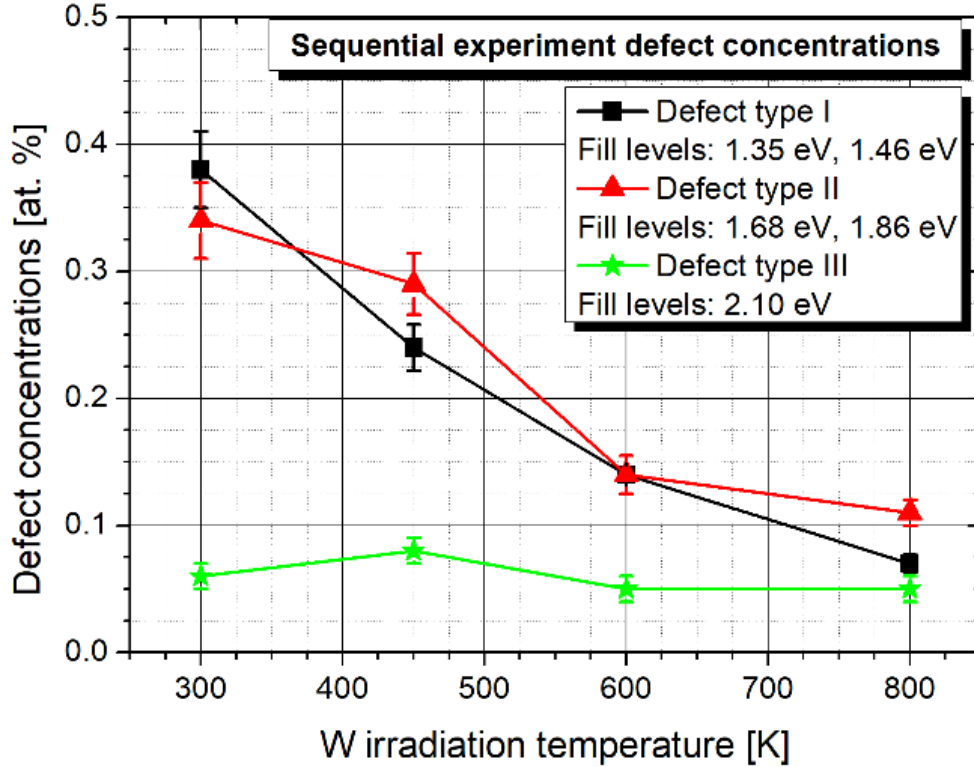

Figure 3: Maximum defect concentration for the three defect types plotted as a function of W-ion irradiation temperature.

The main output of the modelling of the sequential experiment is the saturation concentrations for the three defect types - $n_{i,max}$ - which are plotted in Fig. 3 for the different W irradiation temperatures. The errors of defect concentrations are derived from the errors in D retention that come from the NRA measurement. The results are written out in Tab. 2. We see that defects I and II show similar behaviour with rising temperature, their temperature dependence resembling a linear fall. Their concentrations fall from 0.35 at. % when W irradiating at 300 K to about 0.1 at. % when W irradiating at 800 K. Meanwhile defect type III shows no behaviour with rising W irradiation temperature, being constant at around 0.06 at. %.

It could be speculated that only two distinct defect types are necessary to model the experimental results, as the concentrations of defects I and II are very similar in the entire W irradiation temperature range. To test this hypothesis, we have also tried modelling the experimental results by using a defect type I with four fill-levels (1.35 eV, 1.46 eV, 1.68 eV, 1.86 eV) and a defect type II with a single fill-level with de-trapping energy of (2.10 eV). The fits of the D depth distribution are equally good as expected which is why we focus our analysis on the differences observed in the D desorption spectra. Although we do not

show the comparison between the model and experiment for this choice of fitting parameters we quantified the quality of the fits of the D desorption spectra again by using the reduced chi square. The values of χ^2_{red} are 4.85 for irradiating at 300 K, 5.71 for irradiating at 450 K, 0.57 for irradiating at 600 K and 3.51 for irradiating at 800 K. This implies that merging fill-levels into only one defect significantly worsens the fit of the D desorption spectra. This is due to the fact that the fit is very sensitive to our choice of saturation concentrations, and that several defect types are necessary to replicate the changing ratios of the two D desorption peaks at different W irradiation temperatures. By using only one defect type we were unable to reproduce both the low and high temperature peak at the same time. The fit was only good in the case of irradiating at 600 K, because the saturation concentrations for the original defect I and II were the same at this W irradiation temperature as is shown in Tab. 2.

Table 2: Saturation concentrations $n_{i,max}$ of various defect types as a function of W-ion irradiation temperature. On the bottom also the range over which the de-trapping energies were varied for the different fill levels in order to replicate the experimental D desorption spectra is given. The error column gives the relative errors of the modelled saturation concentrations for the various W-ion irradiation temperatures. They were determined from the accuracy of the NRA measurement. Also the reduced chi squared is presented.

W-ion irrad. temperature [K]	Defect I [at. %]	Defect II [at. %]	Defect III [at. %]	Relative Error	χ^2_{red} [1]
300	0.38	0.34	0.06	4 %	1.70
450	0.24	0.29	0.08	5 %	1.71
600	0.14	0.14	0.05	4 %	0.57
800	0.07	0.11	0.05	6 %	1.10
De-trapping energy [eV]	1.32 – 1.38 1.43 – 1.50	1.66 – 1.69 1.84 – 1.86	2.09 – 2.11		

Returning to Tab. 2 and the fits of the simulation to the sequential W-D experiment, we must note the range of variation of the determined de-trapping energies. We see that the range over which the de-trapping energies were adjusted to fit the D desorption spectra at various W irradiation temperatures is larger in the case of the de-trapping energies attributed to fill-levels of defect type I compared to the range of the de-trapping energies belonging to fill-levels of defect type II. The range of de-trapping energy adjustment can be easier presented in a temperature scale, meaning how much the temperature of a D desorption peak would shift if its de-trapping energy would correspond to the limits of the allowed variation of the de-trapping energy. For a TDS temperature ramp of 3 K/min a change in de-trapping energy of 0.01 eV, corresponds to a shift in the desorption peak of approximately 3 K. This means that the size of the de-trapping energy adjustment range is approximately 20 K for defect type I, and approximately 10 K for defect type II and III.

In Fig. 4 we can see how the desorption from specific fill levels contributes to the experimental desorption spectrum. We see that some of the desorption is negative. This is specific to the fill-level picture of HI trapping and comes from the fact that as the fill level $i + 1$ is de-trapping, the fill level i is filling up. Because when drawing D desorption spectra desorption from a trap is defined as positive, the filling of the lower fill level i is counted as negative. Contribution to the overall D desorption spectrum is plotted with various shades of red for defect type I, with various shades of blue for defect type II and the contribution of defect type III is plotted with green.
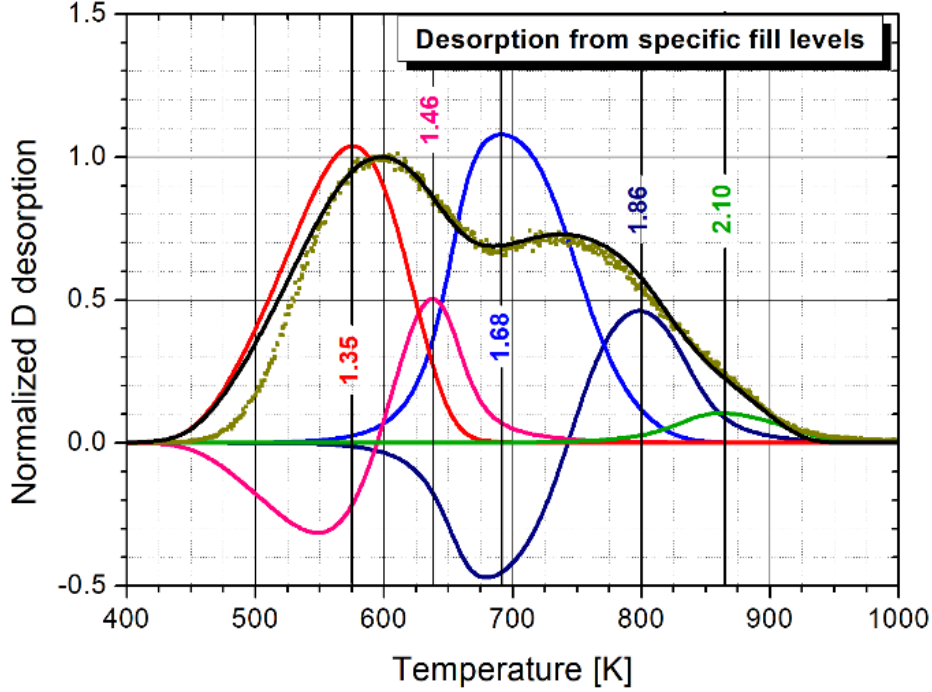
Figure 4: Deconstructing contributions of the specific defect fill levels to the D desorption spectrum of the W irradiated sample at 300 K. De-trapping energies of the fill-levels are represented with vertical lines.

4. 2 Simulation of simultaneous W/D-D experiment

By modelling the sequential W-D experiment, we determined the saturation concentrations $n_{i,max}$ of the defects present in the samples as a function of W irradiation temperature and we also determined the de-trapping energies of their fill-levels. Now we will model the simultaneous W/D-D experiment where the samples were W irradiated at various temperatures by 10.8 MeV W ions, while being simultaneously exposed to 300 eV/D ions. After the four-hour W irradiation procedure was completed the samples were re-exposed to D ions to decorate the created defects. We will try to describe the effect of deuterium presence on defect concentration by changing the stabilization α_i, that was introduced in section 3, while the saturation concentrations $n_{i,max}$ will be kept the same as in their respective sequential W irradiation temperature case. We will also allow for the de-trapping energies to be modified slightly, if necessary to achieve a better fit of the D desorption spectra.

We managed to reproduce the experimental results of the simultaneous W/D-D experiment by changing only α_I and α_{II} during the fitting. This is due to the fact that any possible stabilization of defect type III that could have been seen from the D desorption spectra was overshadowed by the large amount of D desorption from defect type II. Therefore we have set $\alpha_{III} = 0$ as its uncertainty is too large.
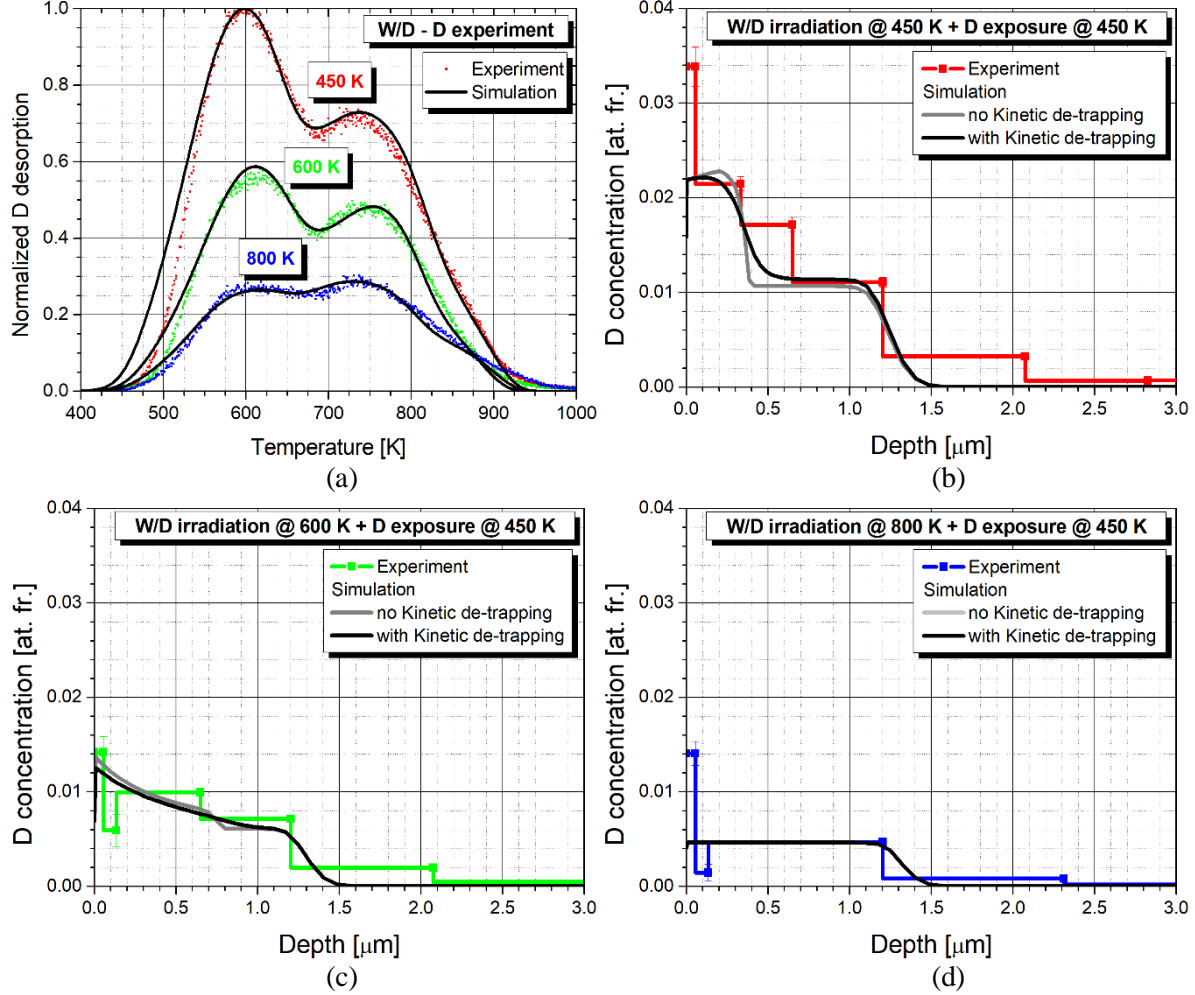
Figure 5: Comparison between the simulation and the experiment of the D desorption spectra for samples simultaneously W irradiated at four different temperatures. The experiments are plotted with connected symbols, while the simulations are plotted with lines. Comparison of D depth profiles between the simulation and the experiment are shown separately for 450 K (b), 600 K (c) and 800 K (d).

The agreement of the simulated D depth profiles with the experimental ones (Fig. 5b-d) is the key information when assessing the success of our stabilization model. In figure 5 we show the comparison of the experimental D desorption spectra (5a) and D depth profiles (5b-d) to the ones provided by the fitting procedure at each W irradiation temperature pair-wise. We observe good agreement, both showing very similar behaviour observed at different temperatures. Namely, the simulation recreates the stepped D depth profile for the 450 K (Fig. 5b) case and the decreasing D concentration with depth in the 600 K (Fig. 5c) case very well while also recreating the flat 800 K (Fig. 5d) case. We could learn from the simulation that the differences in spatial dependence of the D concentration depth profile at different W irradiation temperatures are due to the interplay between D diffusion and D trapping/de-trapping.

Even though we have different D depth distributions at different irradiation temperatures the simulation replicates the experimental D desorption spectra very well, as shown in Fig 5a. The model successfully replicates the two D desorption peak structure seen in the experiment and the different ratios of D desorption in the two D desorption peaks. Again we use the reduced chi square to quantify the quality of the fits in the same manner as in the sequential experiment. These values are 1.37, 1.85 and 0.85 for simultaneous W irradiation/D exposure at 450 K, 600 K and 800 K respectively.

In Figs. 5b-d we also show how the inclusion of the kinetic de-trapping affects the D driven stabilization and changes the D depth profiles. The biggest effect can be seen in the sample simultaneously

W/D-D exposed at 450 K as in that case the D trapping is the strongest and therefore D transport is the slowest without kinetic de-trapping. The inclusion of kinetic de-trapping increases the effectiveness of D de-trapping from fill-levels where it would normally be tightly bound and therefore increases the rate of D transport deeper into the bulk. Therefore, a longer tail is observed extending deeper into the bulk, compared to when no kinetic de-trapping is included. A similar observation can be made in the 600 K case, but the effect is already less pronounced. In the D depth profile of the sample simultaneously W/D-D irradiated at 800 K no difference can be observed, because thermal D de-trapping and diffusion are already very effective at that temperature and therefore almost no additional contribution to the rate of D transport can be seen.

Now that we have completely determined the parameters of the simultaneous W/D-D irradiation experiment we can also model the D depth profiles directly after the four-hour simultaneous W/D irradiation, before the samples were additionally exposed to D ions for 39 hours. The comparison between the simulation and experiment can be seen in Fig. 6. The D flux at the position where these D depth profiles were measured was determined to be $\Gamma_D = 1.3 \times 10^{18}$ D m^{-2}s^{-1} [27]. The fall in D concentrations with rising irradiation temperature that is observed in the experiment is described well by the simulation owing its success mainly to the correct choice of parameters of stabilization α and the de-trapping energies. If no stabilization (α = 0) was included the maximum D concentrations after the simultaneous W/D irradiation would be considerably lower, because less defects would be created. This would also mean the D would penetrate deeper into the samples because there would be less available defects for them to become trapped in. The penetration depth of D is described well in the 600 and 800 K case, but the simulation apparently fails to reproduce the speed of D uptake seen in the 450 K case. In the simulation the D penetrated to a depth of only 0.7 µm deep, while it reached 1 µm in the experiment. This mismatch can be at least partly explained by the fact that the depth resolution of the NRA measurement is approximately 0.5 µm at a depth between 0.5 µm and 1 µm which is why the NRA spectrum fit produced a 0.5 µm wide step with low D concentrations instead of a more realistic narrow and tall step to which the simulation would fit much more nicely. Overall the model behaves well enough considering its limitations, and from this we can state that D presence during simultaneous W/D irradiation stabilizes both defects type I and II through the mechanism of D trapping.
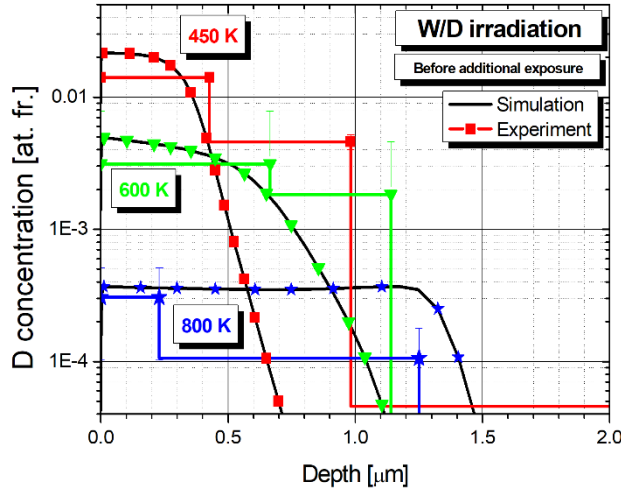

Figure 6: D depth profiles after the simultaneous W ion and D ion exposure, with the W ion flux being 9.72×10^{13} W m^{-2}s^{-1} and D ion flux being 1.3×10^{18} D m^{-2}s^{-1}. The simulation is plotted with lines and the experiment with connected symbols.

The parameters of the simulation relevant to our stabilization model described by equation 2 are written in Table 3. The values of α_I become much larger than 1 in the 600 and 800 K case, making it difficult to understand the stabilization process. This is just a consequence of the fact that at higher temperatures less and less defects are completely filled due to thermal D de-trapping as defined by the occupancy ratio $R_i(x,t) = (n_i(x,t) - n_i^0(x,t))/n_i(x,t)$. As some stabilization is still observed even at 800 K where the

defects are almost completely empty the value of α_i must be sufficiently large to achieve an adequate simulation fit.

Table 3: Simulation parameters relevant to our stabilization model defined in equation 2 as used to describe the W/D-D simultaneous experiment.

W/D temperature	Defect type I			Defect type II			Defect type III		
	$n_{I,max}$	α_I	α_I^*	$n_{II,max}$	α_{II}	α_{II}^*	$n_{III,max}$	α_{III}	α_{III}^*
450 K	0.24	0.66	0.66	0.29	0.29	0.29	0.08	0	0
600 K	0.14	2.37	0.06	0.14	0.39	0.39	0.05	0	0
800 K	0.07	650.63	0.002	0.11	0.44	0.002	0.05	0	0

To transition from the unintuitive α_i parameters that are not bound between 0 and 1 and can therefore not be understood as stabilization probabilities we introduce a new quantity:

$$\alpha_i^* = \alpha_i R_i(x = 0, t \to \infty). \qquad (5)$$

$R_i(x = 0, t \to \infty)$ is defined as the occupancy ratio of the defect type i after equilibrium has been achieved. As equilibrium is achieved quickest at the surface we also define it at x = 0. The equilibrium occupancy ratio mainly depends on the de-trapping energy of the defect fill-levels and on the exposure conditions defined by the exposure temperature and D ion flux. The value of α_i^* is bound between the values of 0 and 1 as the inner parenthesis in equation 2 cannot be negative making it closer in physical meaning to the probability of stabilization of a filled defect as compared to the fitting parameter α_i. The equilibrium occupancy ratio $R_i(x = 0, t \to \infty)$ has been determined from the simulations. The calculated values of α_i^* for the three W/D irradiation temperatures are reported in Tab. 3. The obtained values and dependence of α_i^* on irradiation temperature is drawn in Fig. 7.
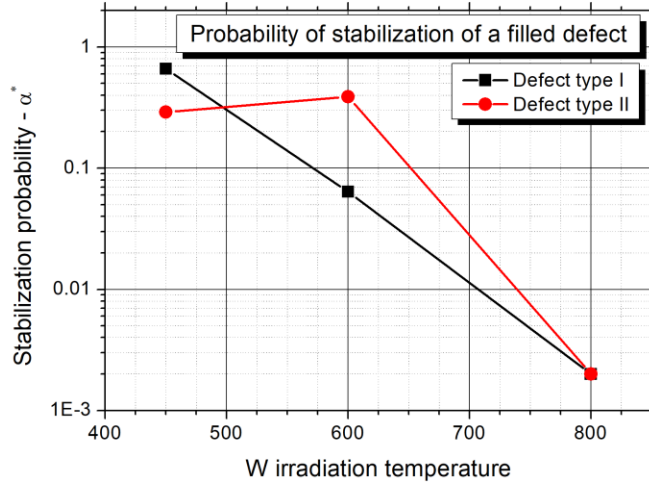

Figure 7: Probabilities of stabilization - α^*- for defect types I and II as a function of W irradiation temperature.

We observe that α_I^* falls exponentially with rising W irradiation temperature (note the logarithmic scale) and is almost zero at the highest W irradiation temperature of 800 K. It is also observed that α_{II}^* experiences a small rise when going from 450 to 600 K as it rises from 0.29 to 0.39. Afterwards it experiences a sharp drop off as it drops almost to zero at 800 K, but it is still not completely zero. This can be attributed to the fact that although the equilibrium D occupation fraction of both defects at high temperatures is small, D still transitionally occupies them as it diffuses through the lattice. During the time the defect is transitionally occupied it can be stabilized just as if it was occupied in equilibrium.

5. Discussion

In the discussion section we will first discuss and try to correlate the determined de-trapping energies in the previous section with the different defect types. After this we will discuss how different defect types are stabilized by the presence of D.

5. 1 Defect identification

Although it is common practice in the community, we wish to stress here that neither the NRA nor the TDS techniques allow the identification of specific defect types unambiguously. Other experimental techniques are available to characterize defect types that are created in an irradiated material. Transmition Electron Microscopy (TEM) can be used to characterize defects such as dislocation lines, loops and other larger structures like voids and bubbles [9], but it cannot detect defects such as single vacancies or vacancy clusters. These can be identified using Positron Annihilation Lifetime Spectroscopy (PALS) [41].

As only the NRA and TDS experimental results can be simulated using our model we will attempt to identify the defects by comparing their de-trapping energies to the ones that can be found in the literature. Through the years a whole spectrum of de-trapping energies was presented for different defect types by many publications. Therefore, we will rather limit ourselves to grouping up some de-trapping energies into energy bands we suspect might belong to the same type of defect, comparing them to our results and also to some DFT calculations of specific defect types.

It is important to mention that relying on the de-trapping energies we get by simulating the TDS measurement has its limitations. Mainly, defects have the potential to evolve during the temperature ramp-up, transforming from one state to another. This means that the type of defects which are de-trapping D during a TDS measurement are not necessarily the same types of defects that were created during the W irradiation process. Unfortunately, no simulation tools are available that could take this effect into account so we must assume that the defects do not evolve during the TDS measurement.

5. 1. 1 Defect type I

We start with defect type I that has two fill levels (1.35 eV, 1.46 eV). Such low de-trapping energies found in the literature are commonly identified as single vacancies. Namely, DFT calculations [14-16] show that vacancies can trap up to 12 HIs with de-trapping energies between 0.5-1.4 eV. Most importantly for our case vacancies that trap one or two HIs have a de-trapping energy in the 1.42 - 1.50 eV range and vacancies that trap 3 HIs have been calculated to have a de-trapping energy of 1.28 - 1.37 eV.

The experimental results in the literature for de-trapping energies that are assumed to belong to vacancies can be summed up into an energy band of 1.2 – 1.5 eV [29, 30, 42, 43]. In addition, Zibrov et al. [44] have irradiated their samples with 10 keV D ions for which they assume to create only vacancy-type defects. After the D-irradiation TDS measurements were made using different temperature ramps. The observed shift in the TDS peaks of the D desorption spectra when using different heating rates can be directly tied to de-trapping energies of vacancies in their case. With this technique they have calculated a de-trapping energy of 1.56 eV corresponding to vacancies.

All of the reported de-trapping energies are in line with the de-trapping energies of defect type I derived from our simulation.

Another important piece of evidence that defect type I is indeed a single vacancy is the experiment by Zibrov [41]. He has irradiated his W samples with 200 keV protons to a fluence of 10^{20} p/m^2 which he assumes creates only Frenkel pairs as primary defects. Using such an energy for the proton irradiation the protons cause displacement damage up to a depth of 1 µm with a damage maximum at 0.7 µm. Using PALS, it was determined that the dominant defect type present in the samples was indeed single-vacancies (relative PALS intensity of 80%) and only a minority were larger defect structures like clusters (relative PALS intensity of 5%). The rest of the signal came from the bulk contribution to the

PALS signal. The comparable displacement damage distribution allows us to compare the D desorption spectra produced in the experiment by Zibrov with our experiment. In the case of Zibrov the D desorption spectra, measured with a heating rate of 15 K/min, consisted of two peaks. A dominant desorption peak is located at 670 K while the peak at 800 K is less pronounced but still clearly visible. In combination with the PALS results the dominant low temperature D desorption peak was attributed to single vacancies. In our experiment the D desorption peaks are located at 600 and 750 K, with a heating rate of 3 K/min. This difference in heating rate creates an approximately 50 K temperature shift of the desorption peaks, which means that both D desorption peaks from both experiments coincide. Therefore, this is another confirmation that defect type I, can be identified as a single vacancy as it is responsible for D desorption in the lower temperature range (see Fig. 4).

5. 1. 2 Defect type II

The identification of defect type II with fill levels (1.68 eV, 1.86 eV) is more ambiguous than in the case of defect type I. Several experiments have reported de-trapping energies similar to the ones found in our simulation ranging from 1.65 – 1.9 eV [6, 28, 30, 31, 37, 40, 43, 45-47].

One option for identification could be small vacancy clusters (usually defined as clusters with less than 15 captured single vacancies). As a crude approximation we relied on the so-called adsorption model of vacancy clusters proposed firstly by Gorodetsky *et al.* [46] and later elaborated on by Ogorodnikova [47]. The adsorption model states that the binding energy of a HI trapped in a vacancy cluster is similar to HI atom chemisorption on the W surface, which becomes more and more accurate as the vacancy cluster grows in size as the number of captured vacancies increases. With this model it was calculated that the binding energy of HIs is 1.4 – 1.6 eV for a vacancy cluster consisting of two vacancies and 1.7 – 1.9 eV for a vacancy cluster consisting of three vacancies. As the de-trapping energy is defined to be the sum of the binding energy and the diffusion energy, the exact de-trapping energies derived from these binding energies written above depend on our choice for the energy associated with diffusion. As in our case the diffusion energy used was 0.2 eV [14] the corresponding de-trapping energy ranges would be 1.6 – 1.8 eV for a vacancy cluster consisting of two vacancies and 1.9 – 2.1 eV for a vacancy cluster consisting of three vacancies. Recently, *ab initio* calculations of D trapping have become available for vacancy clusters in tungsten. Hou *et al.* [48] have used DFT and molecular dynamics calculations to determine the binding energies of H to vacancy clusters with 1-8 captured vacancies (V_1-V_8) for different H/V ratios in the clusters. Assuming a 0.2 eV diffusion energy, they have shown that the majority of fill-level de-trapping energies (for H/V < 3) lie between 1.6 and 1.9 eV, which is a great match to the reported de-trapping energies of our defect type II.

Another possible identification is either jogged dislocation or dislocation loops. Using DFT, Terentyev *et al.* [49] have shown that jogged dislocations have a binding energy of 1.4 eV for 1-3 trapped D atoms. Assuming a diffusion energy of 0.2 eV this would equate to a de-trapping energy of about 1.6 eV. Again using DFT, Xiao *et al.* [50] have shown that dislocation loops have a binding energy between 1.8 eV and 1.6 eV for one and two trapped D atoms, respectively, making the de-trapping energy equal to 2 eV and 1.8 eV, respectively. A. de Backer *et al.* have used DFT and a multi-scale simulation approach to determine the number of H trapped in the Cottrell atmosphere of various dislocation type structures at various exposure temperatures and at various concentrations of solute HIs [51, 52]. They have found de-trapping energies ranging from 0.8 – 1.2 eV for various dislocation structures, number of trapped HIs and for various number of trapped self-interstitial W atoms. Although some of these de-trapping energies are in line with our defect type II fill-level de-trapping energies the typical dislocation areal density found in such samples by TEM analysis [27, 53] is around 10^{14} m^{-2}. This is equivalent to a volumetric concentration of 10^{-4} at.%. As we have determined in our simulation, defect II is responsible for retaining approximately 0.5 at.% of D. Based on these numbers each dislocation would have to trap at least 10^3 D atoms so that one could state that the dislocations contribution to D retention in defect II is non-negligible. According to the calculations by A. de Backer *et al.* dislocations are expected to trap approximately 70 HIs in a dislocation loop consisting of 37 self-interstitial atoms for a HI solute concentration of 10^{-6} at. fr.

[51, 52]. In our experiment the D solute concentration is expected to be in the 10^{-10}-10^{-11} at. fr. range [27]. This means that very few D atoms are expected to be trapped in dislocation loops and that even if there is a contribution of dislocations to the trapping of D in defect type II, it can be considered negligible at an exposure temperature of 450 K for the D ion flux used in [27].

Also as reported in [27] the densities of dislocation structures only decrease by approximately 8 % when the irradiation temperature rises from 300 to 600 K in the sequential W/D experiment, which does not account for the reduction of concentration of the defect type II that has been found in our simulation to be 63%. Considering these facts, we conclude that the defect type II can most likely be identified as a small vacancy cluster.

Based on this conclusion we can determine the possible sizes of vacancy clusters that can survive the W irradiation process. Vacancy clusters that are weakly bound (with respect to irradiation temperature) are expected to dissociate into single vacancies. To determine the binding energies of vacancy clusters that have captured less than 15 single vacancies we can use the calculations by D. R. Mason *et al*. [54] and J. Fikar *et al*. [55]. Assuming a vacancy migration energy of 1.7 eV with corresponding jump frequency of $v_0 = 5.5 \times 10^{12}$ s^{-1} [56] we can calculate a rate of dissociation for differently sized vacancy clusters at our W irradiation temperatures and determine their stability for a four hour W irradiation. From this we calculate that at a temperature of 450 K vacancy clusters with more than 2 captured vacancies are stable, at 600 K clusters with more than 3 captured vacancies are stable and at 800 K clusters with more than 7 captured vacancies are stable.

5. 1. 3 Defect type III

Several simulation and experimental results report similar de-trapping energies to the ones found in our simulation, ranging from 2.0 – 2.2 eV [29-31, 37, 43, 45, 47].

The identification of defect type III with fill level (2.10 eV) is again not completely straight-forward as again several candidates such as large vacancy clusters (more than 15 captured single-vacancies) and various dislocation structures are possible. For similar reasons than in the case of defect type II, any dislocation structures can be ruled out as a possible identity because the density of dislocations as observed in [27, 51] is around 10^{14} m^{-2}, which is too small to account for the defect type III concentrations found in the simulation results section of this paper. Considering this we conclude that defect type III can most likely be identified as a large vacancy cluster.

To determine the theoretically expected de-trapping energies of D from large vacancy clusters we again rely on the adsorption model which leads to the conclusion that large vacancy clusters should behave in a similar fashion to the tungsten surface. Namely, because they are fairly large structures in the W lattice, therefore the HIs captured in them are expected to be in the form of HI molecules. This further means that the de-trapping energy from such a defect is related to the surface kinetics as the molecules must first dissociate before they can re-enter the pristine W lattice. Depending on our choice for the heat of solution the de-trapping energy should be somewhere between $2 – 2.2$ eV which is in good agreement with our de-trapping energy of defect type III. DFT calculations of the energy barrier from the surface to the bulk also report energies between 2.0 and 2.2 eV [15, 16, 57].

In addition, Ryabtsev *et al*. [58] have exposed tungsten samples to 10 keV D ions for which they assume they create only vacancies. After the exposure their samples were annealed at 800 K after which they assume only large vacancy clusters remain. Several TDS measurements with different heating rates were carried out and from the shift of the D desorption peak a de-trapping energy of 2.10 eV was calculated.

5. 2 Mechanisms of defect stabilization

The defect stabilization mechanisms for different defect types are not well known because, to the authors best knowledge, not many atomistic simulations were carried out that would have studied displacement

damage creation in W in the presence of HIs. We hypothesize that vacancy type defects are stabilized by HIs because Frenkel-pair annihilation of a self-interstitial W with a vacancy is less likely if the vacancy has trapped hydrogen HI atoms. This has been explicitly shown by Kato *et al.* [59] on an example of a vacancy containing 6 HIs. They have demonstrated that a vacancy that has trapped 6 HIs does not recombine with a neighbouring <111>-crowdion because a metastable binding state is formed between them.

Stabilization of vacancy clusters by trapped HI atoms is not as intuitive and again little data is available for W. However, molecular dynamics simulations of vacancy clusters interacting with H atoms in bcc-Fe have shown that vacancy clusters that contain H exhibit stronger binding energies of vacancies to the vacancy cluster complex [60]. If we assume that the same mechanism can be considered in W because of its similarity in crystal structure, this would mean that at a certain temperature small vacancy clusters would be less likely to dissociate, increasing their surviving density. The effect of D on binding energies of large vacancy clusters/voids should be negligible because they are already very tightly bound.

5. 3 Probability for stabilization of a filled trap

In section 4, the results of the simulations for both experiments were discussed, where the emphasis was given to the samples that were W irradiated while D was present in the sample. The simulation results fit the experimental results excellently which allows us to discuss how a D filled defect is stabilized. The most interesting quantity that comes out of such a discussion is how many additional defects are created because of the D presence. Let us first discuss how many more additional defects were created for the experimental W fluences used. As can be seen in figure 8 in the 450 K irradiation case approximately 2.5 times the amount of vacancies and 1.5 times the amount of small vacancy clusters are created in the W/D-D experiment compared to the W-D experiment. In the 600 K irradiation case approximately 2.8 times the amount of vacancies and 1.3 times the amount of small vacancy clusters are created in the W/D-D experiment compared to the W-D experiment. In the 800 K irradiation case almost no additional defects were created. Fig. 8a shows the evolution of concentration of the created defect type I (vacancies) for all three W-ion irradiation temperatures with W ion fluence. Fig. 8b shows the same but instead for defect type II (small vacancy clusters). The full lines in both figures show the explicit W fluence dependence in the simultaneous experiment, while the dashed lines of different shades of red (defect type II) and grey (defect type I) show the respective defect saturation concentrations $n_{i,max}$ we have determined in the sequential experiment. The x-axis of both plots are plotted toward each other so one can more easily compare the final saturation concentrations for both defect types. To determine if the defect concentrations found for the experimental W fluences were the saturation defect concentrations at their respective irradiation temperatures, we have decided to extrapolate the current experiment to larger W fluences.

The extrapolation result can be seen in Fig. 8 where we plot the W fluence dependence of defect concentrations near the surface where saturation occurs first. In both figures the non-shaded area shows the defect concentration for W fluences and D ion flux that were used in our experiment. The defect concentrations at the edge of the non-shaded area directly correspond to the defect concentrations present in the sample after the measurement of the D depth profiles as seen in Fig. 5b-d. It can be seen from Fig. 8a and Fig. 8b, that both the vacancies and small vacancy clusters have not saturated yet at 450 K. When irradiating at 600 K only vacancies have not yet achieved saturation. At 800 K both defect types have achieved saturation for the experimentally used W fluences. We wish to stress that the particular saturation behaviour of defect concentrations is specific to the specific D flux used in the experiment, being 1.9×10^{18} D m^{-2}s^{-1}. The grey shaded area represents W fluences where the defect concentrations were extrapolated.
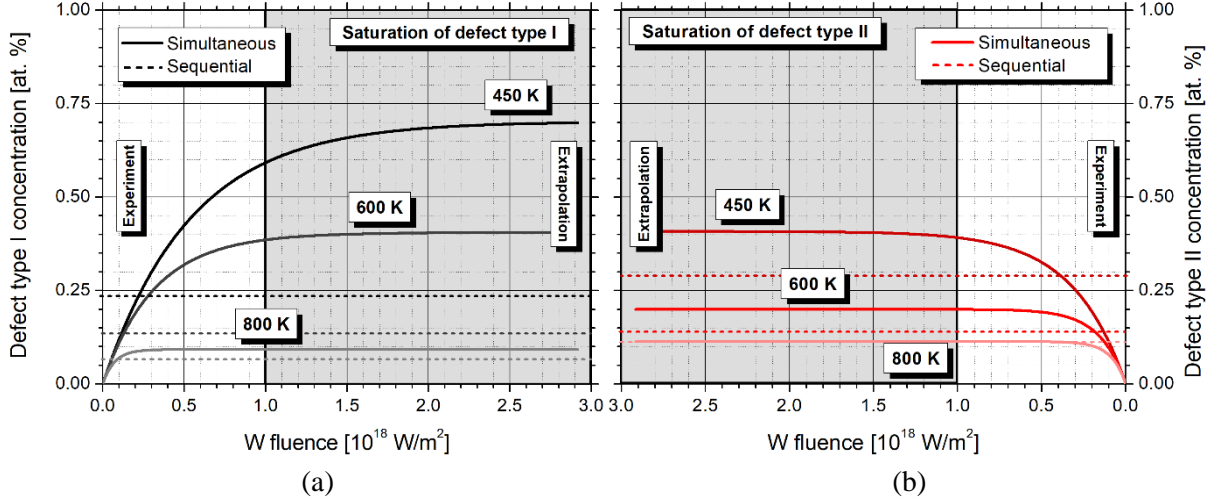
Figure 8: Defect concentration as a function of W fluence. Figure (a) shows the dependence for defect type I while figure (b) shows the dependence for defect type II. The greyed out area signifies extrapolation to higher W fluences that were not achieved in our experiment. The dashed lines represent the saturation concentrations in the sequential experiment while the full lines are the actual fluence dependencies in the simultaneous experiment. The x axis are plotted opposite to each other so one is able to more easily compare the extrapolated concentrations for both defect types.

The extrapolation allows us to determine the final saturated values of defect concentrations (because of D-induced stabilization). From Fig. 8a and Fig. 8b we can see that at 450 K approximately 3 times the amount of vacancies and 1.5 times the amount of small vacancy clusters are created in the W/D-D experiment compared to the W-D experiment. In the 600 K irradiation case approximately 2.9 times the amount of vacancies and 1.3 times the amount of small vacancy clusters are created in the W/D-D experiment compared to the W-D experiment. In the 800 K irradiation case almost no additional defects were created. After determining the final saturated values of defect concentrations we plot them as a function of W irradiation temperature. This can be seen in Fig. 9a. The saturation defect concentrations are much larger in the simultaneous experiment compared to the sequential experiment for both defect types.
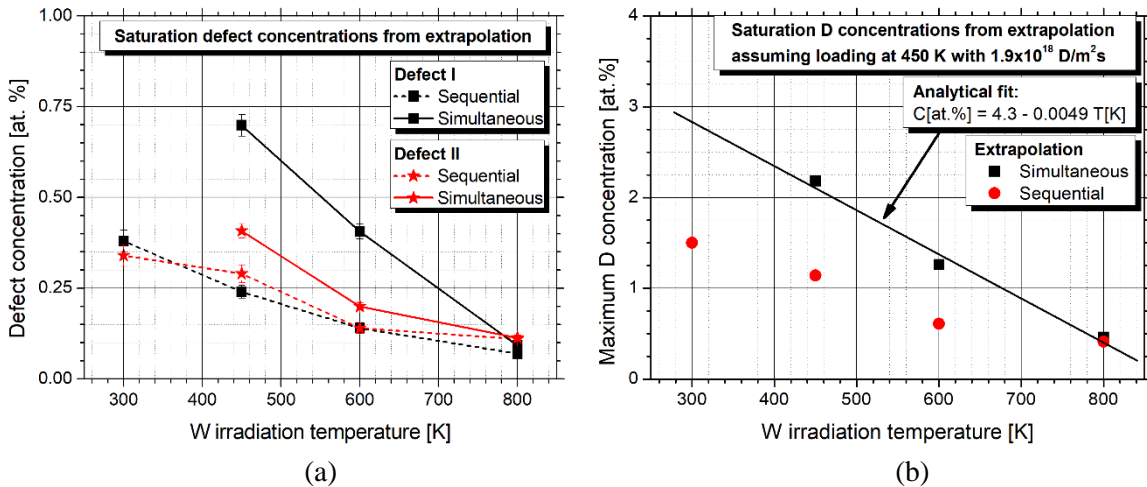

Figure 9: (a) Saturation defect concentrations for defect type I and II as a function of W irradiation temperature. The dashed lines represent the saturation concentrations of the two defects at a certain temperature $- n_{i,max} -$ as derived from the simulation of the sequential experiment and the full lines represent the new saturation levels because of D presence as derived from the extrapolation with the simulation of the simultaneous experiment seen in Fig. 7a and Fig. 7b. (b) The extrapolated defect concentrations are used to determine the extrapolated maximum D concentrations when simultaneous W/D irradiation would occur at specific temperatures and the defects are decorated with ion loading at 450 K with a flux of $\Gamma_D = 1.9 \times 10^{18}$ D $m^{-2}s^{-1}$. They are drawn as black dots. Also an analytical fit is drawn as a black line.

21

By assuming that the same D exposure conditions would be applied to decorate the created defects as used in the experiment, we can calculate the saturation D concentrations that follow from the extrapolated saturation defect concentrations. The assumption of the same D exposure means that the same number of fill-levels and defect types would be occupied by D. Based on this assumption we expect the D concentration to be 2 times higher if W irradiation occurs in the presence of D at 450 K or 600 K compared to if no D is present. When W irradiating at 800 K the amount of displacement damage created is almost completely independent of D presence. This is drawn in Fig. 9b. A linear analytical fit is compared to the simultaneous W/D irradiation extrapolated defect concentration, its equation being $c_{max}\,[at.\%] = 4.3 - 0.0049\,T[K]$. According to the analytical fit, we expect that if the simultaneous W/D irradiation would occur at room temperature, the maximum D concentration would be 2.8 at.%.

From the D depth profiles shown in Fig. 5, another interesting observation can be made, namely, how the additionally created displacement damage is distributed. Concluding from the shape of the experimental D depth profiles (Fig. 5b-d), the entire damaged region is not necessarily near saturation yet in the simultaneous W/D irradiation and D re-exposure experiments. This is especially clear in the case of W irradiation at 450 K, where only around half of the damaged layer is near saturation. From this we conclude that two separate time scales for stabilization are present.

The first is the time scale of displacement damage creation which depends on the displacement damage creation rate $\Gamma_W\eta$ [m^{-3}s^{-1}], the stabilization parameter α_i and $n_{i,max}$. The second time scale is the time scale of D transport into the bulk. This time scale is dominated by the D flux and exposure temperature, but also implicitly depends on the time scale of displacement damage creation as the displacement damage that is created must first be filled by D for it to diffuse further into the bulk.
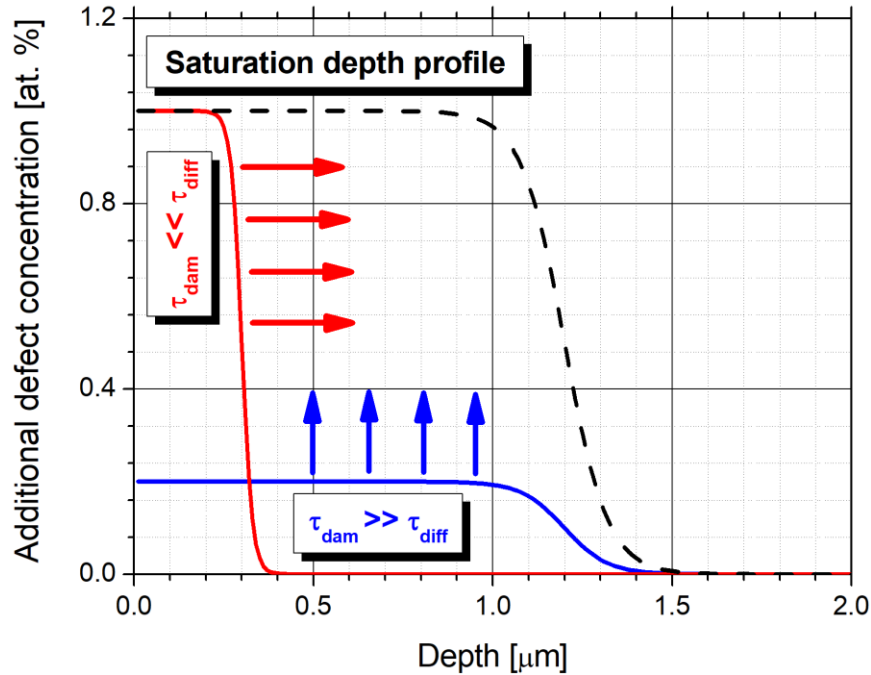

Figure 10: A schematic of how stabilization occurs depending on which time scale is dominant at the beginning of simultaneous displacement damage creation.

The influence of these two time scales on the shape of the D depth profile is schematically presented in Fig. 9. The additional defect concentration has been arbitrarily set to 1 at.% for the ease of illustration. The additional defect concentration is defined as the defect concentration that is created due to D stabilization on top of the expected defect concentration because of W irradiation (sequential W/D experiment) in a hydrogen-free tungsten lattice. If the D diffusion time scale (τ_{diff}) is much faster than the displacement damage creation time scale (τ_{dam}) meaning ($\tau_{dam} \gg \tau_{diff}$) all displacement damage

that is created throughout the entire damaged layer will be immediately filled by D. This further means that stabilization will occur homogeneously in the entire damage layer, as shown by the blue coloured example in Fig. 10. The additional displacement damage created has an exponential saturation dependence on W fluence until saturation, similar to when W irradiating without D presence. This is the case in our 800 K temperature simultaneous W/D-D irradiation experiment shown in Fig. 5d.

The other extreme is when D diffusion is much slower than displacement damage creation ($\tau_{dam} \ll \tau_{diff}$). In that case D penetrates slowly into the sample, which further means that stabilization and saturation occurs in a very narrow region only. Only once the displacement damage in that narrow region is saturated with D, D can penetrate deeper into the sample, where the stabilization again occurs in a narrow region. This means that the stabilization creeps into the sample like a diffusion front. This would mean that the dependence of the additional created displacement damage on W fluence would resemble a square root function, which at larger W fluences has an exponential saturation. This is the case for our 450 K temperature experiment shown in Fig. 5b. In the 600 K case neither of the time scales dominates which is why we see a continuous slope in the entire damage layer in Fig. 5c.

Before this experimental procedure was conducted with ions the very same experimental procedure was conducted but instead of ions, the samples were exposed to 0.28 eV D atoms at an exposure temperature of 600 K. The experiment was later simulated by Hodille *et al.* [26]. A comparison of defect concentrations between both modelling approaches is difficult because in the case of [26] the exposure to atoms was conducted at 600 K instead of the 450 K exposure used here. As a consequence, the defect type I was completely empty and only defect type II and III could be studied. The relatively high re-exposure temperature also meant that some annealing could already occur [8, 9]. In addition to this, Hodille *et al.* chose to simulate the experiment with the classical D-defect interaction picture model instead of the fill-level dependent model. Despite these differences we can still compare the de-trapping energies and the relative behaviour of the defect concentrations as a function of temperature. Hodille *et al.* found two traps with de-trapping energies of 1.83 eV and 2.10 eV. These reported energies are in good agreement with our fill-level two of defect II and defect III, respectively. Hodille *et al.* also found that the saturation concentrations of both traps behaved similarly to our findings. Firstly, the saturation concentration of defect type II (1.83 eV) showed an almost linear fall with rising W irradiation temperature while the defect type III (2.10 eV) showed almost no change. Secondly, the defect type II was stabilized to a relatively large degree (with no stabilization at 800 K, same as here) while defect type III showed a lesser degree of stabilization. Both of these findings are in good agreement with the results of the present work.

It is also important to consider the implications of our damage creation and stabilization model on future fusion tokamak reactor operation. Let us consider ITER as its operational parameters are most well defined. The projected steady state fluxes of HIs are to be on the order of 10^{24} part/m^{2}s at the strike point [1]. The temperature on the plasma facing side of the W mono-blocks is expected to achieve temperatures of around 1300 K and around 500 K on the coolant side [61]. Such high HI fluxes impacting the walls, would mean that despite of the high wall temperature near the plasma facing side a majority of small and large vacancy clusters are expected to be almost completely occupied with at least one D atom, while vacancies will be almost completely empty. As the W material becomes cooler, approaching the coolant facing wall, more and more vacancies will also become occupied. The high HI fluxes will also mean that more fill-levels of the vacancies will be occupied in the deeper regions of the W mono-block, than just the two we have used to describe our experiment. As neutron damage will produce displacement damage throughout the W mono-block we can expect a significant stabilization effect throughout the material, which becomes quite large near the coolant wall surface. Coincidentally, the coolant temperature of 500 K is very near one of our chosen W/D irradiation temperatures of 450 K. This allows us to state that we expect a three-times increase in vacancy concentration and 1.5-times in increase in small-vacancy concentration near the coolant wall. This is a conservative estimate which does not take into account the possibility that with more fill-levels of vacancies being occupied by HIs, one might expect an even higher degree of stabilization. This higher degree of stabilization might be promoted by an (as of yet) unknown dependency of the stabilization probability (α_i^*) on the amount of fill-levels occupied by D.

5. Conclusion

The effect of D presence during displacement damage creation in W irradiated with W ions was studied. A new model for defect creation and stabilization was developed that describes synergistic effects between the displacement damage created by the W ions and the D present in the sample. The model was used to recreate the results of an experiment where samples were first W-ion irradiated and then loaded by D ions – *sequential experiment* – and an experiment where the samples were W-ion irradiated while being loaded by D ions – *simultaneous experiment*. The simulation and experiment showed very good qualitative and quantitative agreement. This was achieved despite significantly decreasing the fitting parameter space by using a fill-level dependent model incorporated in the MHIMS-R code, where several hydrogen isotope atoms can be trapped in one defect. We have decided to use the fill-level dependent model of the D-defect interaction picture because the simulation results and their comparison to the experimental results strongly suggest that the fill-level dependent picture is the correct interaction picture between hydrogen isotopes and defects in the crystal lattice. We have suggested that the dominant three defect types causing significant D retention at 450 K are single vacancies, small vacancy clusters and large vacancy clusters.

The new displacement damage creation and stabilization model's physical meaning is based on the assumption that defects that contain at least one D have a smaller probability of annihilation as compared to D-free defects. By extrapolating the displacement damage created to larger W fluences we have determined the saturation amount of total created displacement damage, which was larger by almost a factor of 2 in the 450 and 600 K damaging case while it was negligible in the 800 K damaging case. By considering how different time scales of D diffusion and displacement damage creation affect additional displacement damage created within the damage zone, we could explain the different shape of the D depth profiles at different W-ion irradiation temperatures on a more conceptual level.

During the fitting process it became apparent to the authors that also the process of kinetic de-trapping introduced in [37] must be included to accurately describe the experimental results as it produced the necessary shape of the final D depth profiles. This is possibly an important aspect of a simultaneous W/D-ion irradiation experiment when the irradiation is done at low temperatures, where thermal D de-trapping is improbable and kinetic de-trapping promotes D diffusion deeper into the sample. The faster D diffusion makes the D diffusion time scale faster, which is an important consideration on how the additional displacement damage created due to stabilization is distributed.

Acknowledgement

References

[1]   V. Chan, R. Stambaugh, A. Garofalo, J. Canik, J. E. Kinsey, J. M. Park, M. Y. K. Peng, T. W. Petrie, M. Porkolab, R. Prater, M. Sawan, JH. P. Smith, P. B. Snyder, P. C. Stangeby and C. P. C. Wong, "A fusion development facility on the critical path to fusion energy," Nucl. Fusion, vol. 51, p. 083019, 2011.

[2] J.-H.You, "A review on two previous divertor target concepts for DEMO: mutual impact between structural design requirements and materials performance," Nucl. Fusion, vol. 55, p. 113026, 2015.

[3] Y. Hatano, M. Shimada, T. Otsuka, Y. Oya, V. Kh. Alimov, M. Hara, J. Shi, M. Kobayashi, T. Oda, G. Cao, K. Okuno, T. Tanaka, K. Sugiyama, J. Roth, B. Tyburksa-Puschel, J. Dorner, N. Yoshida, N. Futagami, H. Watanabe, M. Hatakeyama, H. Kurishita, M. Sokolov and Y. Katoh, "Deuterium trapping at defects created with neutron and ion irradiations in tungsten," Nucl. Fusion, vol. 53, p. 073006, 2013.

[4] E. A. Hodille, E. Bernard, S. Markelj, J. Mougenot, C. S. Becquart, R. Bisson and C. Grisolia, "Estimation of the tritium retention in ITER tungsten divertor target using macroscopic rate equations simulations," Phys. Scr., vol. T170, p. 014033, 2017.

[5] W. R. Wampler and R. P. Doerner, "The influence of displacement damage on deuterium retention in tungsten exposed to plasma," Nucl. Fusion, vol. 49, p. 115023, 2009.

[6] A. Založnik, S. Markelj, T. Schwarz-Selinger, K. Schmid, "Deuterium atom loading of self-damaged tungsten at different sample temperatures," J. Nucl. Mater., vol. 496, pp. 1-8, 2017.

[7] O. V. Ogorodnikova and V. Gann, "Simulation of neutron-induced damage in tungsten by irradiation with energetic self-ions," J. Nucl. Mater., vol. 460, pp. 60-71, 2015.

[8] A. Založnik, S. Markelj, T. Schwarz-Selinger, Ł. Ciupiński, J. Grzonka, P. Vavpetič, P. Pelicon, "The influence of the annealing temperature on deuterium retention in self-damaged tungsten," Phys. Scr., vol. T167, p. 014031, 2016.

[9] O. V. Ogorodnikova, Yu. Gasparyan, V. Efimov, Ł. Ciupiński, J. Grzonka, "Annealing of radiation-induced damage in tungsten under and after irradiation with 20 MeV self-ions," J. Nucl. Mater., vol. 451, pp. 379-386, 2014.

[10] S. Markelj, T. Schwarz-Selinger, A. Založnik, M. Kelemen, P. Vavpetič, P. Pelicon, E. Hodille and C. Grisolia, "Deuterium retention in tungsten simultaneously damaged by high energy W ions and loaded by D atoms," Nucl. Mater. Energ., vol. 12, pp. 169-174, 2017.

[11] E. A. Hodille, X. Bonnin, R. Bisson, T. Angot, C. S. Becquart, J. M. Layet, C. Grisolia, "Macroscopic rate equation modeling of trapping/detrapping of hydrogen isotopes in tungsten materials," J. Nucl. Mater., vol. 467, pp. 424-431, 2015.

[12] K. Schmid, V. Rieger and A. Manhard, "Comparison of hydrogen retention in W and W/Ta alloys," J. Nucl. Mater., vol. 426, pp. 247-253, 2012.

[13] G. Longhurst, "TMAP7 User Manual", INEEL/EXT-04–02352, Idaho Falls, Idaho, Rev. 2, 2008.

[14] N. Fernandez, Y. Ferro and D. Kato, "Hydrogen diffusion and vacancies formation in tungsten: Density Functional Theory calculations and statistical models," Act. Mater., vol. 94, pp. 307-318, 2015.

[15] K. Heinola, T. Ahlgren, K. Nordlund and J. Keinonen, "Hydrogen interaction with point defects in tungsten," Phys. Rev. B, vol. 82, p. 094102, 2010.

[16] D. F. Johnson, E. A. Carter, "Hydrogen in tungsten: Absorption, diffusion, vacancy trapping, and decohesion," J. Mater. Res., vol. 25, pp. 314-327, 2010.

[17] E. A. Hodille, Y. Ferro, N. Fernandez, C. S. Becquart, T. Angot, J.M. Layet, R. Bisson and C. Grisolia, "Study of hydrogen isotopes behavior in tungsten by a multi trapping macroscopic rate equation model," Phys. Scr., vol. T167, p. 014011, 2016.

[18]   K. Schmid, U. von Touissant and T. Schwarz-Selinger, "Transport of hydrogen in metals with occupancy dependent trap energies," J. Appl. Phys., vol. 116, p. 134901, 2014.

[19]   J. Bauer, "Hydrogen isotope exchange in tungsten at low temperatures, Ph.D," Technical university of Munich, 2018.

[20]   E. Wakai, T. Sawai, K. Furuya, A. Naito, T. Aruga, K. Kikuchi, S. Yamashita, S. Ohnuki, S. Yamamoto, H. Naramoto, S. Jistukawa, "Effect of triple ion beams in ferritic/martensitic steel on swelling behavior," J. Nucl. Mater., vol. 307–311, pp. 278–282, 2002.

[21]   E. Wakai, K. Kikuchi, S. Yamamoto, T. Aruga, M. Ando, H. Tanigawa, T. Taguchi, T. Sawai, K. Oka, S. Ohnuki, "Swelling behavior of F82H steel irradiated by triple/dual ion beams," J. Nucl. Mater., vol. 318, pp. 267–273, 2003.

[22]   T. Tanaka, K. Oka, S. Ohnuki, S. Yamashita, T. Suda, S. Watanabe, E. Wakai, "Synergistic effect of helium and hydrogen for defect evolution under multi-ion irradiation of Fe–Cr ferritic alloys," J. Nucl. Mater., vol. 329–333, pp. 294–298, 2004.

[23]   M. Ando, E. Wakai, T. Sawai, H. Tanigawa, K. Furuya, S. Jitsukawa, H. Takeuchi, K. Oka, S. Ohnuki, A. Kohyama, "Synergistic effect of displacement damage and helium atoms on radiation hardening in F82H at TIARA facility," J. Nucl. Mater., vol. 329–333, pp. 1137–1141, 2004.

[24]   E. Wakai, M. Ando, T. Sawai, K. Kikuchi, K. Furuya, M. Sato, K. Oka, S. Ohnuki, H. Tomita, T. Tomita, Y. Kato, F. Takada, "Effect of gas atoms and displacement damage on mechanical properties and microstructures of F82H," J. Nucl. Mater., vol. 356, pp. 95–104, 2006.

[25]   J. Marian, T. Hoang, M. Fluss, L. L. Hsiung, "A review of helium–hydrogen synergistic effects in radiation damage observed in fusion energy steels and an interaction model to guide future understanding," J. Nucl. Mater., vol. 462, pp. 409–421, 2015.

[26]   E.A. Hodille, S. Markelj, T. Schwarz-Selinger, A. Založnik, M. Pečovnik, M. Kelemen and C. Grisolia, "Stabilization of defects by the presence of hydrogen in tungsten: simultaneous W-ion damaging and D-atom exposure," Nucl. Fusion, vol. 59, p. 016011, 2019.

[27]   S. Markelj, T. Schwarz-Selinger, M. Pečovnik, A. Založnik, M. Kelemen, J. Bauer, P. Pelicon, W. Chromiński and L. Ciupinski, "Displacement damage stabilization by hydrogen presence under simultaneous W ion damage and D ion exposure," Nucl. Fusion, vol. 59, p. 086050, 2019.

[28]   M. Pečovnik, S. Markelj, A. Založnik and T. Schwarz-Selinger, "Influence of grain size on deuterium transport and retention in self-damaged tungsten," J. Nucl. Mater. vol. 513, pp. 198-208, 2019.

[29]   M.H.J. 't Hoen, M. Mayer, A.W. Kleyn, H. Schut and P.A. Zeijlmans van Emmichoven, "Reduced deuterium retention in self-damaged tungsten exposed to high-flux plasmas at high surface temperatures," Nucl. Fusion, vol. 53, p. 043003, 2013.

[30]   O. V. Ogorodnikova, S. Markelj and U. von Toussaint," Interaction of atomic and low-energy deuterium with tungsten pre-irradiated with self-ions," J. Appl. Phys., vol. 119, p. 054901, 2016.

[31]   Yu. M. Gasparyan, O. V. Ogorodnikova, V. S. Efimov, A. Mednikov, E. D. Marenkov, A. A. Pisarev, S. Markelj and I. Čadež, "Thermal desorption from self-damaged tungsten exposed to deuterium atoms," J. Nucl. Mater., vol. 463, pp. 1013-1016, 2015.

[32]   O. V. Ogorodnikova, J. Roth and M. Mayer, "Ion-driven deuterium retention in tungsten," J. Appl. Phys., vol. 103, p. 034902, 2008.

[33]   G. Duesing, W. Sassin, W. Schilling, H. Hemmerich, "Defect production during low-temperature electron irradiation. Part I. Spontaneous recombinations and recombinations of frenkel defects by subthreshold recoil events," Cryst. Lattice Defects 1, vol. 70, pp. 55-68, 1969.

[34]   V. Kh. Alimov, Y. Hatano, B. Tyburksa-Püschel, K. Sugiyama, I. Takagi, Y. Furuta, J. Dorner, M. Fußeder, K. Isobe, T. Yamanishi and M. Matsuyama, "Deuterium retention in tungsten damaged with W ions to various damage levels," J. Nucl. Mater., vol. 441, pp. 280-285, 2013.

[35]   O. V. Ogorodnikova, B. Tyburska, V. Kh. Alimov and K. Ertl, "The influence of radiation damage on the plasma-induced deuterium retention in self-implanted tungsten," J. Nucl. Mater., vol. 415, pp. S661-S666, 2011.

[36]   http://www.srim.org/, 29. 7. 2019.

[37]   T. Schwarz Selinger, J. Bauer, S. Elgeti and S. Markelj, "Influence of the presence of deuterium on displacement damage in tungsten," Nucl. Mater. Energ., vol. 17, pp. 228-234, 2018.

[38]   K. Schmid, J. Bauer, T. Schwarz-Selinger and S. Markelj, "Recent progress in the understanding of H transport and trapping in W," Phys. Scr., vol. T170, p. 014037, 2017.

[39]   P. W. Tamm and L. D. Schmidt, "Interaction of H_2 with (100) W. I. Binding States," J. Chem. Phys., vol. 51, p. 5352, 1969.

[40]   J. Guterl, R. D. Smirnov and S. I. Krasheninnikov, "Revisited reaction-diffusion model of thermal desorption spectroscopy experiments on hydrogen retention in material," J. Appl. Phys., vol. 118, p. 043302, 2015.

[41]   M. Zibrov, "The influence of radiation, mechanical, and plasma-induced damage on deuterium retention in tungsten," Ph.D. thesis, Technischen Universität München, Germany (2018).

[42]   O. V. Ogorodnikova, J. Roth and M. Mayer, "Deuterium retention in tungsten in dependence of the surface conditions," J. Nucl. Mater., vol. 313-316, pp. 469-477, 2003.

[43]   M. Shimada, G. Cao, Y. Hatano, T. Oda, Y. Oya, M. Hara, P. Calderoni, "The deuterium depth profile in neutron-irradiated tungsten exposed to plasma," Phys. Scr., vol. T145, p. 014051, 2011.

[44]   M. Zibrov, S. Ryabatsev, Yu. Gasparyan and A. Pisarev, "Experimental determination of the deuterium binding energy with vacancies in tungsten," J. Nucl. Mater., vol. 477, pp. 292-297, 2016.

[45]   E. A. Hodille, A. Založnik, S. Markelj, T. Schwarz-Selinger, C.S. Becquart, R. Bisson and C. Grisolia, "Simulations of atomic deuterium exposure in self-damaged tungsten," Nucl. Fusion, vol. 57, p. 056002, 2017.

[46]   A. E. Gorodetsky, A. P. Zahkarov, V. M. Shaparov and V. Kh. Alimov," Interaction of hydrogen with radiation defects in metals," J. Nucl. Mater., vol. 93-94, pp. 588-593, 1980.

[47]   O. V. Ogorodnikova, "Fundamental aspects of deuterium retention in tungsten at high flux plasma exposure," J. Appl. Phys., vol. 118, p. 074902, 2015.

[48]   J. Hou, X.-S. Kong, X. Wu, J. Song and C. S. Liu, "Predictive model of hydrogen trapping

and bubbling in nanovoids in bcc metals," Nat. Mater., vol. 18, pp. 833-839, 2019.

[49]   D. Terentyev, V. Dubinko, A. Bakaev, Y. Zayachuk, W. van Renterghem and P. Grigorev, "Dislocations mediate hydrogen retention in tungsten," Nucl. Fusion, vol. 54, p. 042004, 2014.

[50]   W. Xiao and W. T. Geng, "Role of grain boundary and dislocation loop in H blistering in W: A density functional theory assessment," J. Nucl. Mater., vol. 430, pp. 132-136, 2012.

[51]   A. de Backer, D. R. Mason, C. Domain, D. Nguyen-Manh, M.-C Marinica, L. Ventelon, C. S. Becquart and S. L. Dudarev, "Hydrogen accumulation around dislocation loops and edge dislocations: from atomistic to mesoscopic scales in BCC tungsten," Phys. Scr., vol. T170, p. 014073, 2017.

[52]   A. de Backer, D. R. Mason, C. Domain, D. Nguyen-Manh, M.-C Marinica, L. Ventelon, C. S. Becquart and S. L. Dudarev, "Multiscale modelling of the interaction of hydrogen with interstitial defects and dislocations in BCC tungsten," Nucl. Fusion, vol. 58, p. 016006, 2018.

[53]   W. Chrominski, L. Ciupinski, P. Bazarnik, S. Markelj and T. Schwarz-Selinger. 2019. "TEM investigation of the influence of dose rate on radiation damage and deuterium retention in tungsten," Mater. Charact., vol. 154, pp. 1–6, 2019.

[54]   D. R. Mason, D. Nguyen-Manh and C. S. Becquart, "An empirical potential for simulating vacancy clusters in tungsten", J. Phys. Condens. Matter, vol. 29, p. 505501, 2017.

[55]   J. Fikar, R. Schäublin, D. R. Mason and D. Nguyen-Manh, "Nano-sized prismatic vacancy dislocation loops and vacancy clusters in tungsten", J. Phys. Condens. Matter, vol. 29, p. 505501, 2017.

[56]   K.-D. Rasch, R. W. Siegel and T. Ahlgren, "Quenching and recovery investigations of vacancies in tungsten," *Philos. Mag. A,* vol. 41, pp. 91-117, 1979.

[57]   A. Moitra and K. N. Solanki, "Adsorption and penetration of hydrogen in W: A first principles study," Comput. Mater. Sci., vol. 50, pp. 2291-2294, 2015.

[58]   S. Ryabtsev, Yu. Gasparyan, M. Zibrov, A. Shubina and A. Pisarev, "Deuterium thermal desorption from vacancy clusters in tungsten," NIMB, vol. 382, pp. 101-104, 2016.

[59]   D. Kato, H. Iwakiri, Y. Watanabe, K. Morishita and T. Muroga," Super-saturated hydrogen effects on radiation damages in tungsten under the high-flux divertor plasma irradiation," Nucl. Fusion, vol. 55, p. 083019, 2015.

[60]   E. Hayward and C. Deo, "Energetics of small hydrogen–vacancy clusters in bcc iron," J. Phys. Condens. Matter., vol. 23, p. 425402, 2011.

[61]   https://www.iter.org/mach/CoolingWater, 9. 8. 2019